UNIVERSITY OF
BATH

Link to publication

University of Bath

Modelling of as Manufactured Geometry for Prediction of Impact and Compression after Impact Behaviour of Variable Angle Tow Laminates

Thi D Dang[1], Stephen R Hallet[1], Byung Chul Kim[1], Yann Le Cahain[1], Richard Butler[2] and Wenli Liu[3]

Advanced Composite Centre for Innovation and Science (ACCIS), University of Bristol, Queen's Building, University Walk, BS8 1TR, UK

Abstract

The development of variable angle tow (VAT) technology has attracted growing attention in recent years due to its strong potential for structural tailoring. However, the full details of the failure mechanisms of VAT laminates have been as yet unknown, and the design complexity also requires use of numerical analysis and novel techniques for VAT composites. This paper addresses the two main problems for use of VAT laminates in design. Firstly, a mathematical model is presented to build a 3-D VAT model which exactly captures the features of as manufactured VAT laminates. Secondly, impact and compression after impact (CAI) models using 3-D detailed finite element analyses are presented to predict the failure behavior of VAT laminates including delamination evolution and crack propagation. Results obtained from the impact and CAI models are validated against experimental data.

Keywords

[1]ACCIS, Department of Aerospace Engineering, University of Bristol
[2]Department of Mechanical Engineering, University of Bath, UK
[3]Department of Aerospace Engineering, Cranfield University, UK

Corresponding author:
Thi D Dang and Stephen R Hallett. ACCIS, Department of Aerospace Engineering, University of Bristol, Queen's Building, University Walk, BS8 1TR, UK. Email: thid.dang@bristol.ac.uk (Thi Dang); stephen.hallett@bristol.ac.uk (Stephen Hallett)

Introduction

Composite laminates are widely used in the aerospace industry, the structure of which normally consists of layers stacked at different fibre orientation angles, often limited to 0, ±45, and 90 degrees. When limiting each ply to a single orientation of straight fibres, the designer is unable to fully utilize the directional material properties offered by advanced composites for structures that possess stress states that vary as a function of location within the laminate. Allowing the fibres to curve within the plane of the laminate gives a tailoring possibility to account for a non-uniform stress state, as well as providing other structural advantages such as the alteration of principal load paths. Particular application of such technology is found in buckling driven designs in the aerospace sector. Tailoring of the tow paths can allow for increased buckling resistance and a more graceful transition into the post-buckling regime. NASA researchers are looking to reduce the weight of the future fuselage structures by 25%, and technologies such as curved fibre paths will help to accomplish this goal. Because of the strong potential of tow-placed laminates for structural tailoring, the development of variable angle tow (VAT) technology has attracted growing attention in recent years,[1-7] it has also led to the birth of a new branch of research in laminated composite materials. However, the design complexity requires use of numerical analysis and novel techniques for modelling and predicting the responses of such structural composites. Gürdal and Olmedo,[8] Tatting and Gürdal[9] have presented a simple method for modelling tow paths, which resulted in the formulation of a tow steered ply definition with a minimum number of parameters. The simple formulation is necessary for the attractiveness of the concept, and to allow for fast optimization algorithms to produce the best manufacturable structural design. As well as stiffness and buckling, damage resistance and tolerance are extremely important design drivers in aerospace structures. Thus, the advantages in terms of tailored stiffness and buckling resistance that VAT laminates can bring, they should also be assessed in terms of their behavior under impact and compression after impact, which are two important industry standard tests.[10-11] For the latter analytical and numerical methods provide a convenient and cost effective solution.

Structural composites display a wide variety of failure mechanisms as a result of their complex structure and manufacturing processes, which include fibre failure, fibre matrix debonding, matrix cracking, buckling and delamination. Delamination, that is, the debonding between adjacent laminae, is the most significant single failure mode in laminated composites since it significantly reduces the strength of the laminate. The greatest reduction is that of the compressive strength which may be up to 40–60% of that of an undamaged structure.[12-13] Delaminations are often induced by different types of impacts, of which low-velocity impact is considered the most dangerous, because it is very difficult to detect in a routine visual inspection.[14] Therefore, the study of low-velocity impact and compression after impact (CAI) behaviour of laminated composites is one of the most important problems in the design of composite structures. To date, a large number of publications on this subject have been published and were mainly devoted for predicting damage observed in experimental work.[14-23] The main focus of research on the low-velocity impact and CAI behaviour has been on simple configurations of straight fibre laminates with limited fibre orientation angles of 0 and 90 degrees. For the damage analysis of curvilinear fibre laminates, Lopes, Gurdal and Camanho[24] carried out first-ply failure analyses on variable-stiffness panels, optimised for buckling, by using a continuum damage mechanics-based failure model. Analyses were extended into the postbuckling progressive damage behaviour and final structural failure[25] due to accumulation of fibre and matrix damage. However, only failure modes at ply-level were considered. Failure modes of delamination at interfaces and the interaction between matrix cracks and delamination, which have shown to be important, were not addressed.

The first study on the prediction of delamination and crack propagation in VAT laminates was carried out by Dang and Hallett.[26] An explicit finite element analysis using bilinear cohesive law-based interface elements and cohesive contacts was employed to predict the impact and CAI behaviour of VAT laminates with constant thickness. This study provided useful information for the understanding of the interaction

between material orientation, matrix cracks, delaminations and local/global buckling modes. The VAT laminates considered in the current paper are manufactured using the Continuous Tow Shearing (CTS) technique.[27] The CTS head has a built-in device to partially impregnate a dry tow with a resin film, which can produce a semi-impregnated tow material. Since the tow is partially impregnated, fibres within the tow can easily slide against each other providing higher shear flexibility than that of conventional slit-tapes. The tow produced is supplied to a pinch device located at the head tip with a small clearance from the substrate, and placed on a substrate by a compaction shoe after passing through a small shearing gap. When the head moves along the tow width by making the compaction shoe slide on the tow while supplying the tow material, the tip of the pinch device changes the position of one of two shear boundaries, which can shear the tow material within the shearing gap. The sheared tow is placed when the head moves along the tow length. In actual operation, since the head moves in both the lateral and laydown directions at the same time, the shearing process can occur continuously. When the tow trajectory is shifted laterally to the tow laydown direction to create the variable orientation, the CTS technique produces a VAT laminate with thickness variation. The thickness change due to tow shearing is directly related to the shear angle. The advantage of this manufacturing method is that VAT laminates are produced without the process-induced defects of the conventional automated fibre placement (AFP) as well as without any tow overlap, and fibre discontinuity. However, modeling and predicting the behavior of VAT laminates with thickness variation is difficult due to the variation of both fibre angle and thickness. Delamination damage at interfaces and cracks in composite plies induced by low-velocity impacts can be predicted in 3-D laminate finite element models using cohesive interface elements and cohesive contacts. This work requires a 3-D VAT model in computer simulation, which poses a significant challenge due to the complex fibre paths and manufacturing method. It is crucial to make sure that interlaminar interfaces in the model are fully in contact with each other during the impact analyses.

The objective of the current paper is to develop a numerical model of as manufactured VAT laminates in the computer simulation and investigate the impact and CAI behavior of VAT laminates. Firstly, we present a methodology for the modelling of three dimensional-VAT laminates with thickness variation using a mapping technique, which allows a VAT laminate with a reference thickness to be transformed to a VAT laminate with spatial coordinate-dependent thickness, whilst still allowing surfaces at the interfaces to fully contact each other. The idea behind this technique is to build a mathematical model, which exactly captures the features of as manufactured VAT laminates. The second motivation of the current paper is to study the impact and CAI behaviour of VAT laminates. Based on the previous work of the authors,[26] explicit detailed finite element models using bilinear cohesive law-based interface elements and cohesive contacts in Abaqus/Explicit[28] are applied to investigate the impact and CAI behaviour of VAT laminates with delamination and crack growth. As for the prediction of delamination, cohesive elements present a number of advantages over other modelling approaches e.g. capacity to investigate both initiation and growth of damage, incorporating both strength and fracture mechanics theories. Another added advantage is that the use of interface elements does not require the assumption of any initial damage size or propagation direction.[29-30] Furthermore, computationally expensive remeshing procedures are not required to capture delamination propagation. For these reasons, interface elements are used to predict the onset and growth of delamination in this study. The bilinear constitutive law, which is possibly the most widely adopted cohesive traction-displacement curve, was used in the current paper because of its simplicity to describe the interfacial behaviour under mode I and mode II loading.[30] Here interface elements are used to predict the onset and propagation of delamination at interfaces, while cohesive contacts are used to predict the onset and propagation of matrix cracks. Two models were built for predicting the behaviour of VAT composite laminates with consideration of delamination and crack growth. Firstly, an impact model is developed to predict the damage induced by low-velocity impacts. Secondly, a compression after impact (CAI) model is presented to predict the in-plane compression behaviour of the delaminated VAT laminate.

Initial delaminations and cracks for the CAI model are accurately taken from the damage predictions of the impact model. Results obtained from the impact and CAI models are validated with experimental data to demonstrate the effectiveness of the current models for predicting the extent of impact damage and subsequent compression strength, especially to enhance the understanding of the failure mechanism of VAT laminates.

The paper is organized as follows. In the first section, a brief description of the design of the VAT laminate used in this work through optimisation under buckling constraint is given. The objective of optimization is to minimize panel mass whilst satisfying buckling and manufacturing constraints. Also in this Section, the manufacture of the VAT laminates using the Continuous Tow Shearing technique is presented. A mathematical model of the as manufactured VAT laminate for computer simulation is developed. In the second section, the modelling of low-velocity impact tests is performed, with numerical results and experimental data being compared in detail for validation of the method. The third section covers the modelling of compression after impact (CAI) tests, in which details of CAI model, numerical results and discussions are presented. Finally, a summary and conclusions are presented.

Design, manufacture and modelling of VAT laminates

Optimization of VAT laminates under buckling load constraints

In this section the minimum-mass optimization strategy[6] used for the design of the VAT laminates in this study subject to buckling and manufacturing constraints using the infinite strip analysis is summarised. The two industry standard tests for impact[10] and compression after impact[11] are used in the current paper for VAT laminates, thus the size of panels is set by the ASTM standard,[10-11] which is 100 *mm* x 150 *mm*. An Infinite Strip Method (ISM) is employed to model the VAT panels and linear buckling analyses are

performed based on the model.[31] In this method, the VAT panel is divided into a number of strips of equal width and the fibre angle θ_i of each strip is free to vary whilst satisfying buckling constraints. As each strip has a constant fibre angle, the fibre angle within the VAT panel is constant along the length direction y of the panel but variable along the width direction x of the panel (see Figure 1). Anti-symmetry is imposed about the panel centreline, as shown in Figure 1. The fibre path $\theta(x)$ is represented as the fibre angle θ_i in each strip (see Figure 1). The eigenvalue analysis uses a transcendental stiffness matrix derived from the solution of the governing differential equations of the constituent strips. The number of strips for buckling analyses was checked to ensure mesh convergence whist maintaining computational efficiency.

The Continuous Tow Shearing (CTS) technique[27] can achieve a minimum radius of tow path of 30 mm. When the tow is sheared, the thickness is changed according to the shear angle. Assuming the fibre volume of the tow element is not changed, the function of $f(t_0, \theta)$ is used to denote the change of the sheared tow thickness t according to the initial tow thickness t_0 before shearing and the tow shear angle θ. The sheared tow thickness t is given by

$$t = t_0 / cos\theta \tag{1}$$

The formula is singular when $\theta = 90^0$, but practically θ cannot be equal to 90 degrees for manufacturability reasons. The tow angles which the tow head of the prototype CTS machine can handle is

$$0^° \leq \theta \leq 75^° \tag{2}$$

The objective function of the optimization is to minimize panel mass whilst satisfying buckling and manufacturing constraints. The design variables are the layer thickness and fibre angle in each strip. The design problem is a constrained minimization problem as follows

$$
\begin{aligned}
\text{Minimize} \quad & m \\
\text{Subject to} \quad & F(\lambda) \geq 1 \\
& t_i = f(t_0, \theta_i) \\
& \theta_i^l \leq \theta \leq \theta_i^u
\end{aligned}
\tag{3}
$$

where m is panel mass, $F(\lambda)$ is the critical buckling load factor over all half-wavelengths λ, and θ_i is the fibre angle in each strip. The initial tow thickness t_0 before shearing is set as a reference thickness from which the sheared tow thickness t_i is calculated according to equation (1). θ_i^l and θ_i^u are the lower bound and upper bound of the fibre angle in each strip. The stack sequence is defined in the input file. Both initial thickness and fibre angle of each strip are the design variables. As equation (3) shows, the thickness of each strip t_i is dependent on the initial tow thickness t_0 and the fibre angle θ_i. Due to the nature of continuous optimization, the optimum result of layer thickness is rounded up or down to a closest integer number of layers according to t_0.[6]

A feasible directions method[37] is applied to solve the constrained optimization problem. The sensitivity of $F(\lambda)$ to the variation of θ_i and t_i in each strip is used to direct the gradient-based optimizer to achieve feasibility and minimize the total laminate thickness. The basic approach in the feasible directions method is to select a starting point, satisfying all the constraints, and move in a feasible direction at each iteration to improve the objective value. The method requires the calculation of the sensitivity of the objective function and constraints with respect of the design variables. The output from this analysis was to produce a VAT laminate with optimised tow trajectories whose manufacture is described in the next section.

Manufacturing VAT laminates using the Continuous Tow Shearing technique

VAT composite specimens with special angle variations and a stacking sequence of $[\theta_1\theta_1/_1\theta_1/_2\theta_1/_2]_s$ were manufactured by the CTS technique.[27] Figure 2(a) and Figure 2(b) show the fibre trajectories on the actual specimen geometry and the non-linear fibre angle variations for the θ_1 and θ_2.

These actual fibre paths were obtained by interpolating vertices of a polyline, which follows the piecewise angle variation of the optimized ISM, with a cubic polynomial function. The cubic functions corresponding to the fibre paths were as follows:-

$$
\begin{aligned}
y_1 &= -0.0005x^3 - 0.0071x^2 - 0.6027x \quad \text{with} \quad -50 \le x \le 0 \\
y_1 &= -0.0005x^3 + 0.0071x^2 - 0.6027x \quad \text{with} \quad 0 \le x \le 50 \\
y_2 &= -0.0005x^3 - 0.0017x^2 - 0.2554x \quad \text{with} \quad -50 \le x \le 0 \\
y_2 &= -0.0005x^3 + 0.0017x^2 - 0.2554x \quad \text{with} \quad 0 \le x \le 50
\end{aligned}
\tag{4}
$$

The functions of fibre angle variation were obtained by differentiating the above functions in order to consider accurate fibre angle distribution of the manufactured VAT panel.

As shown in Figures 3(a) to (c), VAT prepreg was produced on release films for each ply first, and then manually stacked to form the finished laminate thickness. A flat tool plate and a flexible silicone rubber sheet were used for the bottom and top surfaces respectively for autoclave curing, which produced an uneven but smooth top surface of the specimen and a flat bottom surface. 24K dry carbon tows (Tenax-E IMS65, Toho Tenax Co. Ltd., EU) were used with 80 gsm resin films (MTM49-3, ACG, UK). The specimens were cured at 0.6 MPa and 135°C for 90 minutes in the autoclave. Figure 3(c) shows the cured specimen whose edges were trimmed using a diamond cutting wheel. The thickness variation was investigated through CT scanning and image analysis, which was almost the same along the vertical direction (shifting direction) and matched well with equation (1).[32]

Modelling of as manufactured geometry of VAT laminates

Building three dimensional models for the impact and CAI tests on VAT panels using detailed finite element analyses has proved very challenging, because VAT laminates not only have the in-plane variation of fibre angle but also variation in thickness. As mentioned above, thickness variation occurs due to the shear deformation of dry tows. Therefore, each ply of the VAT laminate will be a smooth curvilinear surface, which leads to some difficulties in computer simulation using commercial finite element analysis software, for instance Abaqus.[28] In commercial FEA software, smooth curvilinear surfaces are actually created by discrete spatial nodes, thus in a VAT laminates each ply contacts each other through contacts of their nodes. When modelling the impact and CAI behaviour of VAT laminates using cohesive elements for delamination between the plies, each composite layer needs to be created separately with the cohesive elements inserted into the interfaces afterwards. Therefore, it is crucial to make sure that the ply surfaces in the models are fully in contact with each other during the analyses. The upper surface of the bottom layer is used as an initial base to create next layer, and so on the upper surface of each created layer is again used as a base to another consecutive layer which is above the base. For VAT laminates with cracks, as a crack path is created in a ply and coincident nodes are used along the crack path, the same crack path is also created for all other plies, but for plies on which the crack path is expected as an inactive crack, doubled nodes will be removed and cohesive contact is also inactive. In this way, we can create different meshes between plies. The problem for creating manufactured geometry of VAT laminates has been resolved by using a mapping technique coded in MATLAB, which allows a VAT laminate with a reference thickness to be transformed to a VAT laminate with spatial coordinate-dependent thickness (see Figure 4), whilst still allowing surfaces at the interfaces to fully contact each other. The idea behind this technique is to build a mathematical model, which exactly captures the features of as manufactured VAT laminates.

Denoting M as a geometric object consisting of a set of composite and cohesive layers M_k ($k = 1\ldots n$) with reference thickness t_k^o for a conventional laminate with constant thickness, $\tilde{M}$ as a geometric object consisting of a set of layers $\tilde{M}_k$ for a VAT laminate with thickness variation, and n is the number of layers in the VAT laminate, thus we have

$$M = \bigcup_{k=1}^{n} M_k; \quad \tilde{M} = \bigcup_{k=1}^{n} \tilde{M}_k \tag{5}$$

Denoting ∂M_k^l and ∂M_k^u the lower surface and the upper surface of the layer M_k respectively. $\partial \tilde{M}_k^l$ and $\partial \tilde{M}_k^u$ analogically are the lower surface and the upper surface of the layer $\tilde{M}_k$. Let (X, Y, Z) be the global coordinate system, and $\left(X_k, Y_k, Z_k \right)$ be the local coordinate system of the layer M_k, respectively. In our definition, the plane $\left(X_k, Y_k \right)$ lies in the lower surface, and h_k is the distance between the local coordinate and the global coordinate. The layer M_k is mapped into the layer $\tilde{M}_k$ via the mapping function f_k as

$$
\begin{aligned}
&f_k : M_k \rightarrow \tilde{M}_k \\
&f_k = \tilde{h}_k \Big|_{on\ \partial \tilde{M}_{k-1}^u} + \frac{t_k^o}{\cos \theta_k} \\
&\text{with } \partial \tilde{M}_k^l = f\left(\partial M_{k-1}^u \right) \text{ for } \forall\ X, Y \in \mathbb{R}^2 \\
&\qquad f\left(M_k \right) \bigcap f\left(M_{k-1} \right) = \varnothing
\end{aligned}
\tag{6}
$$

where $\tilde{h}_k$ is the height of the upper surface of the layer $\tilde{M}_{k-1}$.

In practice, we can represent equation (6) in the discretization form as the following. Denote m, number of elements through thickness for the layer M_k, so we have $m+1$ surfaces on which nodes are defined. In

each surface, we have p rows and q columns, the nodal matrix for the surface is $\mathbf{N}^{surface}_{(p,q)}$. Thus, the nodal

matrix for layer M_k will be

$$\mathbf{N}_k = \mathbf{N}^{surface}_{(p,q)} \otimes \{1 \quad 1 \quad .... \quad 1\}^T_{(1,m+1)} \tag{7}$$

Coordinate Z for each element $N_k(i,j)$ of the matrix $\mathbf{N}_k$ will be

$$\tilde{Z}_k(i,j) = \tilde{Z}_{k-1}(i,j)\Big|_{on\ \partial \tilde{M}^u_{k-1}} + \frac{Z_k(i,j)}{\cos\left[\theta_k(i,j)\right]} \tag{8}$$

where θ_k in equations (6, 8) are the fibre angle and of the tow path defined in equation (1). When the

optimization work is performed, the optimal fibre path for each lamina is obtained as shown in equation

(4), because of fibre variation, material properties in the finite element model are varied from element to

element. In order to handle this issue, a code was written in Matlab to define the material properties for the

VAT composite laminates. Here, the computation of fibre angle is considered at the centroid of each

element. However, the computation of the fibre angle at nodes is also necessary to determine the Z

coordinate in equation (8).

The output from the Matlab code is a mesh and material orientations for use in Abaqus/Explicit . The

constant thickness VAT laminate model has been validated through benchmark examples.[8, 26] Here the as

manufactured VAT laminate model with variable thickness is compared against experimental results for

impact and CAI tests as described in the following sections.

Low-velocity impact modelling

The impact model to predict the damage induced by low-velocity impacts is presented in this section. A detailed guideline for modelling of VAT laminates is given in the earlier work[26] that provided useful information for the understanding of the interaction between material orientation, matrix cracks and delaminations. In this work,[26] parameters defining the cohesive behaviour of the interface are identified by comparison of numerical results with experimental data, different features such as cohesive interface element model parameters, surface-based cohesive behaviour, mass scaling, material density, element size and meshing issues are also investigated in detail using Abaqus/Explicit.[28] Bilinear cohesive law-based interface elements are used to predict the onset and growth of delamination while cohesive contacts are used to predict the onset and propagation of matrix cracks.[30]

The model uses the optimised fibre angles of $[\theta_1/-\theta_1/-\theta_2/\theta_2]_s$ with fibre paths shown in equation (4). The panel size and test configuration is as specified in the ASTM drop weight impact standard;[10] 100 *mm* x 150 *mm*, simply supported by a steel plate having a rectangular opening 75 *mm* x 125 *mm* in size, and impacted by a mass of 6.3524 kg having a hemispherical indenter of 16 mm in diameter. The impact test setup under the Instron Dynatup 9200 Drop Weight Impactor and 3-D impact model are shown in Figure 5. The VAT laminate with thickness variation is mapped from a laminate with reference thickness t_o=0.13 *mm* for each composite layer using the mathematical model as described above, and the laminate with reference thickness has a similar stacking sequence to the optimized VAT laminate. The $\pm\theta_1$ and $\pm\theta_2$ sublaminates are each modelled through their thickness with two C3D8R reduced integration solid elements, while COH3D8 cohesive elements are inserted at the two interfaces between layers with different orientation ($+\theta_1/-\theta_1$, $-\theta_1/-\theta_2$ and $-\theta_2/\theta_2$ interfaces), and in this case, there are such six interfaces. A thickness of 15 *μm*, which is maintained throughout the study, is assumed for the cohesive interface, laminate and interfacial properties are shown in Table 1.

Table 1. Laminate and cohesive properties used in the simulation[*].

Laminate properties		Cohesive properties	
E_{11} (GPa)	163	G_{IC} (J/m^2)	200
$E_{22} = E_{33}$ (GPa)	6.8	$G_{IIC} = G_{IIIC}$ (J/m^2)	809
$G_{12} = G_{13}$ (GPa)	3.4	N (MPa)	40
G_{23} (GPa)	2.4	$S=T$ (MPa)	170
$V_{12} = V_{13}$	0.28	k_{I} (GPa/mm)	160
	0.4	$k_{\mathrm{II}} = k_{\mathrm{III}}$ (GPa/mm)	57
V_{23}			

[*]Data is taken from Ref. (33-35).

To simulate the initiation and growth of the major intralaminar tensile matrix crack, typically developing along the fibre direction in the lower block of layers of the VAT laminate,[26] a potential matrix-crack (coincident nodes joined by cohesive contact) is inserted in the bottom layer, passing through the origin at centre of the plate. This tensile crack is assumed to lie along the fibre orientation. The crack path is defined by equation (4) and was explicitly included in the mesh in the bottom layer using a Matlab pre-processing script, cohesive contacts are used for the interaction between the two crack surfaces.[26] The cohesive properties in Table 1 are used for modelling both the tensile crack and delaminations. An element size of 0.5 *mm* by 0.5 *mm* (on the laminate plane) is used in the region of the damaged area for the laminate, while cohesive elements with the same size of 0.5 *mm* by 0.5 *mm* are used for the whole cohesive layer, the cohesive elements are attached to the laminate elements using *Tie Constraints* in Abaqus[28] and the meshes are dissimilar.[26, 30]. The fine mesh region on the laminate plane is 20 *mm* x 40 *mm*. The impactor was modelled as a rigid analytical surface associated with a pointwise mass. An impact energy (*E=6J*) is simulated by imposing the appropriate velocity to the impactor at the moment of contact, as computed from

$V = \sqrt{\dfrac{2E}{m}} = 1.3744 m/s$, E is the impact energy and $m=6.3524$ kg is the mass of the impactor, the bottom

support steel plate is a rigid body discretised with R3D4 rigid elements. Contact between the impactor and

the laminate specimen is simulated by the general contact algorithm in Abaqus/Explicit,[28] which uses a

penalty enforcement contact method. This contact formulation is also applied between the different

composite layers when the cohesive elements become fully damaged and are removed from the mesh.

Friction with a coefficient of 0.3 is introduced between all the contacting surfaces. The analyses were

carried out on a parallel computing system of 8 CPUs with two 3.2 GHz Pentium D processors.

Figure 6 shows comparison of predicted and experimental force-time curve. It can be seen that the model

gives a representation in comparison with the experiment. Reasonable estimates are obtained for the

maximum impact force (3049.2 N) and the impact duration (10.802 ms). The difference of the maximum

impact force and the impact duration between the current impact model and the impact test is 7.34% and

11.87% respectively. The introduction of damageable cohesive elements allows dissipation of energy (due

to delamination). As a consequence the numerical specimen becomes less stiff. Therefore, the numerical

model will become more flexible, and thus the time of impact increases. The duration of impact depends

upon various factors such as the impact energy, lay–up sequence and thickness of the specimen.

Moreover, in our impact experiment, the translation in the z direction at four points on the impact face of

the VAT laminate was controlled as seen in Figure 5(a), this may make the experimental specimen more

stiff. The specimen with higher bending stiffness shows a smaller impact duration. Delamination initiation

happens at 1.827 ms (see Figure 7) after contact takes place, at interface 1 (see Figure 7(b)). The

maximum impact force obtained from the impact test is lower than that predicted by the impact model,

this trend was also observed by Dang and Hallett,[26] the observed difference in the current study is 7.34%

and is more evident than that of the VAT laminate with constant thickness.[26] It may be because there are

more matrix cracks generated in the experiment compared to what is included in the model, as was observed in experiments on larger VAT laminates.[36] Such matrix cracks are arranged in a complicated pattern that would be extremely difficult to predict and be beyond the capability of the current damage models.

The predicted results in terms of delamination evolution are presented in Figure 7. It is seen that delamination propagation happened at interfaces 1, 3, 5 and 6 (see Figure 7(c) to (f)). Damage morphology in each of these interfaces is viewed from the impact face of the VAT laminate (see Figure 7(a)). Delamination started at t =1.827 *ms* at interface 1, this was followed at interface 3 at t=1.856 *ms* and after that at interface 5 at t=1.914 *ms* and then delamination finally occurred at interface 6. Figure 8 shows delamination obtained from the experiment of the impact test using C-scan, damage morphology in Figure 8(a) is viewed from the back face of the VAT laminate, whilst damage morphology in Figure 8(b) is viewed from the impact face of the laminate. The colour scale in Figure 8 (b) indicates depth with blue representing near the impact face followed by green, yellow and red representing the deepest delamination. The delaminations with red and yellow colours in Figure 8(a) are the same delaminations viewed from the back with blue and green colours in Figure 8(b) respectively (but rotated by 90°).

From a comparison of delamination morphologies between the impact model and the experiment, it is apparent that the analysis predicts which interface has delamination well. Overall the delamination shapes at the corresponding interfaces matched well. The difference in the maximum size between the model and the experiment is 30.9%, 3.54%, 9.6% and 8%, at interfaces 1, 3, 5 and 6 respectively. It is apparent that the effect of fibre orientation and the tensile crack on delamination shape and size is very significant. In both the experiment and the impact modelling, the delamination obtained at the interfaces tends to propagate along the fibre direction of the lower ply of the interface. The effect of matrix cracks on the predicted delamination propagation is significant.

16

Figure 9 shows the largest tensile crack in the bottom composite layer predicted by the impact model compared to the impact test. We can see that the tensile crack in the bottom layer can be predicted well by the insertion of a single crack into to the mesh and its length agrees well with the test. The difference between the crack length obtained from the impact model and that from the experiment is about 2.5%. The tensile crack in both the experiment and the impact model propagated along the fibre orientation of the bottom layer (θ_1 direction). The tensile crack propagation started at t=0.522 *ms* which was much earlier than the starting time of delamination. The tensile crack was thus instrumental in the delamination initiation at interface 1. The delamination shape is thus guided by the tensile crack. It would be possible to include matrix cracks in each ply, but the computational cost would become extremely expensive and was beyond the capability the current computer system. The single large tensile crack at the back face seems to be sufficient in this case to influence the delamination propagation. It should be noted that only one experimental result could be obtained here due to the complexity of VAT laminate manufacture and its prototype nature. The manufacturing technique developed is however fully automated for laydown of the curved tows and so is highly repeatable. The single experimental results is thus still considered representative of typical behaviour, within the usual experimental scatter for composites testing. The experimental and modelling work of different VAT specimens under impacts with different impact energies is ongoing and will be reported in future publications.

Compression after impact modelling

The CAI behaviour of the impacted and unimpacted VAT laminate is studied in this section. The CAI model for the compression behaviour prediction of the impacted VAT laminate accurately accounts for details of the delaminations and cracks induced by low-velocity impacts from the impact model. A uniform compressive displacement in the *x* direction is applied at *x* =a/2 with x=-a/2 held constant. The sides of the

plate were simply supported at $y = \pm b/2$ and not constrained in-plane (see Figure 10). Thus, the boundary conditions of the laminates are:

$$u = w = 0 \text{ at } x = -a/2$$
$$u = u_o, w = 0 \text{ at } x = a/2 \qquad (9)$$
$$w = 0 \text{ along the line } y = \pm b/2 \text{ and } z = 0$$

The mechanical properties of the laminates and interfacial properties are shown in Table 1. The morphology of delaminations and cracks induced in the impact simulations is accurately taken from the impact model as the starting point for damage in the CAI simulation.

Similarly to the impact model the CAI model is run in Abaqus/Explicit using C3D8R reduced integration solid elements for the plies. Cohesive elements, COH3D8, with element size 0.5 *mm* by 0.5 *mm,* are inserted in selected regions of the two interfaces between layers of different orientation. This was only where un-failed cohesive elements from the impact analysis remained, representing no delaminations (see Figure 7). Failed cohesive elements from the impact analysis, representing delaminations, are deleted for the CAI simulation using a Matlab script and replaced by a contact formulation.[28] The tensile crack (see Figure 9) generated in the impact model is kept and still assumed to propagate along the fibre orientation. Cohesive contacts are used to simulate the crack propagation in the CAI models. Two damage analyses of compression behaviour were performed as follows: Firstly, a simulation of compression behaviour is performed for the unimpacted VAT laminate, no initial damage due to the impact is included in this simulation. Secondly, CAI simulation is performed for the impacted VAT laminate. In this CAI model, initial damage is taken from the impact model (see Figures 7, 9); delamination and crack growth are considered in the CAI model. Results obtained from the CAI models of the impacted and unimpacted VAT laminate are validated with the experimental data, respectively.

18

Figure 11 shows the force-displacement curves of the unimpacted and impacted VAT laminates obtained from the CAI test and the CAI modelling. It can be immediately noted that the result of the force-displacement curve obtained from the CAI modelling for both the unimpacted and impacted VAT laminate is almost the same. This observation is also found from the CAI test for both the unimpacted and impacted VAT laminate, although, the stiffness obtained for the impacted VAT laminate is slightly lower than that obtained for the unimpacted VAT laminate due to the damage induced by the impact. This difference in stiffness is not present in the analyses. From these observations, we can conclude that damage induced by the impact does not affect the CAI strength which requires some further investigation of the damage mechanisms as discussed below. The model gives a reasonable estimate of the initial stiffness (see segment *0-P1* in Figure 11) and the maximum CAI strength in comparison with those obtained from the experiment. The difference of the CAI strength between the experiment (*F*=56.2 *KN*) and the CAI modelling (*F*=50 *KN*) is about 11%. On the experimental force-displacement curves, the non-linear region in the early stage of the CAI test was caused by bedding in of the contact surfaces between the test rig and the machine cross-head, which is typically observed in compression tests. On the force-displacement curve from the model, *P1* (*u*=0.699 *mm*, *F*=47.379 *KN*) denotes the point of the delamination initiation, *P2* (*u*=0.716 *mm*, *F*=40.648 *KN*) the point after the delamination has propagated a short way, *P3* (*u*=0.849 *mm*, *F*=5.06 *KN*) the point after major delamination propagation, and *P4* (*u*=1.8 *mm*, *F*=4.731 *KN*) denotes the end point of the simulation. The delamination propagation at the different interfaces and deformed shapes of model are shown in Figure 12.

From Figure 12 it is immediately obvious that in the impacted case it is not the impact damage which is controlling the failure process and that the delamination pattern is almost identical to the undamaged pattern. The delaminations started from corners of the interface 5 at *P1* in Figure 12 with the unimpacted

panel starting marginally before the impacted one. It is observed that after the delamination starts, the delaminations happened at all interfaces from their corners, and mainly propagated diagonally to the loading direction (see Figure 12). The precise sequence of damage events is difficult to determine experimentally since once damage initiates it propagates very suddenly. In the post failure specimens it is possible to observe clear delaminations at the corner locations as predicted by the model (see unimpacted panel in Figure 13). The overall damage in the experimental cases is however more extensive than predicted, particularly in the case of the impact damaged plate where subsequent delamination propagation seems to interact with the impact damaged area. The fact that the experimental impacted VAT laminate has the same CAI strength as the undamaged laminate strongly indicates that the impact damage is not the source of failure initiation. In all simulations the fibre direction compressive stress was monitored. At $P1$ (delamination onset), the maximum fibre direction compressive stress of 623.3 MPa is obtained in the impacted VAT laminate, which is well below fibre compression strengths of typical carbon/epoxy laminates. This is further evidence that the delamination failures started before other failure modes. Therefore although the models presented did not explicitly include a progressive fibre failure model, it is shown that this is not necessary and that the delamination failures predicted are the dominant failure mode.

The compression behaviour can be explained as follows. The optimisation for minimum mass whilst satisfying the buckling constraint has caused a variation in fibre angle such that the low angle load bearing fibres are located towards the constrained edges of the panel and the unsupported centre of the panel has buckling resistant fibre orientations greater than 45 degrees. Whilst this is beneficial for the buckling resistance of the panel it also means that the compression load is not evenly distributed across the width of the panel, increasing the risk of material and delamination failure at the highly loaded panel edges. This issue is compounded by the VAT laminate thickness distribution (see Figure 3 and Figure 5(b)), which is directly related to the shear angle (see equation 5). Here the thickness along two edges of the structure is

~4.1 *mm* (see Figure 10), which is much greater than that (~1.2 *mm*) at the middle of the structure. Thicker plies are known to increase the propensity for delamination, based on simple fracture mechanics arguments. Thus, whilst having the thickest, most heavily load bearing part of the structure at the specimen edge is good for the buckling behaviour; it has also been the cause of failure through delamination in the compression test, which the model has accurately predicted.

It should be noted that the outcome of the compression after impact would be different if constraints on strength and damage tolerance were involved in the design optimization of VAT laminates. The optimization of steered fibres for multiple constraints on buckling, damage tolerance and strength is a very difficult problem, due to the occurrence of many local optima and a large number of design variables.[38] At this early stage of the current work, the VAT panel was optimized with the buckling constraints only since improved buckling behaviour is one of the key benefits of using VAT panels. Future work will conduct the optimization of VAT laminates using the framework for the optimal design of complex structures with multiple constraints under multiple-load cases.[38]

Summary and conclusions

In this paper the modelling of as manufactured VAT laminates and their failure mechanisms under impact and compression after impact have been studied. A VAT panel has been designed, based on the optimisation of mass for a required buckling load and its manufacture briefly presented. A method to build a mathematical model of the 3-D VAT laminate which exactly captures the features of the as manufactured configuration was presented. Finally, the impact and CAI models were run to predict the impact and CAI behaviour of the VAT laminates using an explicit finite element analysis. In the models, bilinear cohesive law-based interface elements and cohesive contacts were used to model the delamination and crack growth. The obtained results were validated with the experimental data. Some remarks on this work can be summarized as follows.

(1). In the impact model, all of the delaminations propagated in the fibre direction of the layer below their interfaces. The results obtained from the impact model are found to agree well with the experimental data.

(2). In the CAI model, the delaminations started from the corners of the VAT laminates. The existence of damage originating from the impact at the centre of the VAT laminate did not affect the force-displacement curves and the sublaminate buckling modes. The results obtained from the CAI modelling were validated with the experimental data, and showed that the CAI modelling can give a good estimate of the CAI strength.

Results from the present study show differences from previous work[26], which considered only constant thickness plies. To obtain the level of correlation shown here it is that necessary to model the as manufactured condition (thickness variation) in the analysis, which would have otherwise not correctly captured load distribution and delamination failure in the compression load case. It also highlights the need to consider all possible failure modes in the design stage of determining the fibre orientations for VAT laminates. In most cases the perceived benefit of the variable angle tows is the increase in buckling resistance, but as has been shown this may in turn lead to other undesirable failure modes. This first work considering the failure of VAT laminates has focussed on the industry standard ASTM impact and CAI tests and validation of an initial set of numerical models. Due to the redistribution of load this may not be the most important case to investigate since an impact in heavily loaded edge region may cause severe knockdowns. To this end a new specimen configuration has been designed (see Ref. 36) and future work will investigate the CAI behaviour of VAT laminates with initial damage induced by impacts in the thicker regions of low fibre angles, multiple-matrix cracks will also be considered in these impact models.

Conflict of interest

None declared.

References

1. Hyer M and Charette R. Use of curvilinear fiber format in composite structure design. *AIAA J* 1991; 29:1011-1015.

2. Weaver PM, Potter KD, Hazra K, Saverymuthapulle M and Hawthorne MT. Buckling of variable angle tow plates: From concept to experiment. In: *50th AIAA/ASME/ASCE/AHS/ASC Structures, Structural Dynamics and Materials Conference*, Palm Springs, California, May, 2009, AIAA 2009-2509.

3. Ghiasi H, Fayazbakhsh K, Pasini D and Lessard L. Optimum stacking sequence design of composite materials Part II: Variable stiffness design. *Compos Struct* 2010, 93: 1–13.

4. Wu Z, Raju G and Weaver PM. Buckling analysis of VAT plate using energy method. In: *53rd AIAA/ASME Structures, Structural Dynamics and Materials Conference,* Hawaii, April 2012.

5. Raju G, Wu Z, Kim BC and Weaver PM. Prebuckling and buckling analysis of variable angle tow plates with general boundary conditions. *Compos Struct* 2012, 94: 2961–2970.

6. Liu W and Butler R. Buckling Optimization of Variable-Angle-Tow Panels Using the Infinite-Strip Method. *AIAA J* 2013; 51(6): 1442-1449.

7. Ribeiro P, Akhavan H, Teter A and Warminski J. A review on the mechanical behaviour of curvilinear fibre composite laminated panels. *J Compos Mater* 2013, 1-17. DOI: 10.1177/0021998313502066.

8. Gurdal Z and Olmedo R. In-Plane Response of Laminates with Spatially Varying Fiber Orientations: Variable Stiffness Concept. *AIAA J* 1993; 31: 751-758.

9. Tatting BF and Gurdal Z. *Design and manufacture of elastically tailored tow placed plates*. NASA/CR 2002- 211919, 2002: 1-14.

10. ASTM D 7136/D 7136M–05. Standard test method for measuring the damage resistance of a fiber-reinforced polymer matrix composite to a drop-weight impact event. In: *Annual Book of ASTM Standards*. ASTM International, West Conshohocken, PA, 2005.

11. ASTM D 7137/D 7137M-05. Standard test method for compressive residual strength properties of damaged polymer matrix composite plates. In: *Annual Book of ASTM Standards*. ASTM International, West Conshohocken, PA, 2005.

12. Soutis C and Curtis PT. Prediction of the prediction of the post-impact compressive strength of CFRP laminated composites. *Compos Sci Technol* 1996; 56: 677-684.

13. Davies GAO, Hitchings D, Besant T, Clarke A and Morgan C. Compression after impact strength of composite sandwich panels. *Compos Struct* 2004; 63:1–9.

14. De Freitas M and Reis L. Failure mechanisms on composite specimens subjected compression after impact. *Compos Struct* 1998; 42: 365-373.

15. Abrate S. *Impact on composite structures*. Cambridge University Press, 1998.

16. Lammerant L and Verpoest I. Modeling of the interaction between matrix cracks and delaminations during impact of composites plates. *Compos Sci Technol* 1996; 56: 1171-1178.

17. Moura MFSF and Goncalves JPM. Modelling the interaction between matrix cracking and delamination in carbon–epoxy laminates under low velocity impact. *Compos Sci Technol* 2004; 64: 1021–1027.

18. Aymerich F, Dore F and Priolo P. Prediction of impact-induced delamination in cross-ply composite laminates using cohesive interface elements. *Compos Sci Technol* 2008; 68: 2383–2390.

19. Aymerich F, Dore F and Priolo P. Simulation of multiple delaminations in impacted cross-ply laminates using a finite element model based on cohesive interface elements. *Compos Sci Technol* 2009; 69: 699–1709.

20. Suemasu H, Sasaki W, Ishikawa T and Aoki Y. A numerical study on compressive behavior of composite plates with multiple circular delaminations considering delamination propagation. *Compos Sci Technol* 2008; 68: 2562–2567.

21. Moura MFSF, Goncalves JPM, Marques AT and Castro PMST. Modeling compression failure after low velocity impact on laminated composites using interface elements. *J Compos Mater* 1997; 31: 1462-1479.

22. Aoki Y, Suemasu H and Ishikawa T. Damage propagation in CFRP laminates subjected to low velocity impact and static indentation. *Adv Compos Mater* 2007; 16: 45–61.

23. Sanchez-Saez S, Barbero E, Zaera R and Navarro C. Compression after impact of thin composite laminates. *Compos Sci Technol* 2005; 65: 1911–1919.

24. Lopes C, Gurdal Z and Camanho P. Variable-stiffness composite panels: Buckling and first-ply failure improvements over straight-fibre laminates. *Comput Struct* 2008; 86: 897–907

25. Lopes CS, Camanho PP, Gurdal Z and Tatting BF. Progressive failure analysis of tow-placed, variable-stiffness composite panels. *Int J Solids Struct* 2007; 44: 8493–8516.

26. Dang TD and Hallett SR. A numerical Study on Impact and Compression after Impact Behaviour of Variable Angle Tow Laminates. *Compos Struct* 2013, 96: 194–206.

27. Kim BC, Potter K and Weaver PM. Continuous tow shearing for manufacturing variable angle tow composites. *Compos Part A* 2012, 43:1347–1356.

28. Simulia Corp. *Abaqus Theory Manual, Version 6.9-EF*. Providence, RI, USA; 2009.

29. Harper P and Hallett SR. Cohesive zone length in numerical simulations of composite delamination. *Eng Fract Mech* 2008; 75: 4774-4792.

30. Dang TD and Hallett SR. Impact and Compression after Impact Behavior Prediction of Variable Angle Tow Composites. In: *ASC 27th Annual Technical Conference of the American Society for Composites*. October 2012, Arlington, Texas.

31. Williams FW, Kennedy D, Butler R and Anderson MS. VICONOPT: program for exact vibration and buckling analysis or design of prismatic plate assemblies. *AIAA J* 1991; 29: 1927–1928.

32. Kim BC, Weaver PM and Potter K. Manufacturing characteristics of the continuous tow shearing method for manufacturing of variable angle tow composites. *Compos Part A* 2014, (accepted).

33. ACG product catalogue no. PDS1059/11.09/11.

34. Barikani M, Saidpour H and Sezen M. Mode-I interlaminar fracture toughness in unidirectional carbon-fibre/epoxy composites. *Iran Polym J* 2002, 11: 413-423.

35. Saidpour H, Barikani H and Sezen M. Mode-II interlaminar fracture toughness of carbon/epoxy laminates. *Iran Polym J* 2003, 12: 389-400.

36. Rhead AT, Butler R, Liu W, Kim BC and Hallett SR. Compression after impact strength of a buckling resistant, tow steered panel. In: *19th International Conference on Composite Materials*, Montreal, 2013.

37. Vanderplaats GN. *CONMIN— a Fortran Program for Con- strained Function Minimisation, User's Manual*. NASA TM-X-62282, 1973.

38. Dang TD, Kapania RK, Slemp WCH, Bhatia M and Gurav SP. Optimization and postbuckling analysis of curvilinear-stiffened panels under multiple-load cases. *J Aircraft* 2010, 47: 1656-1671.
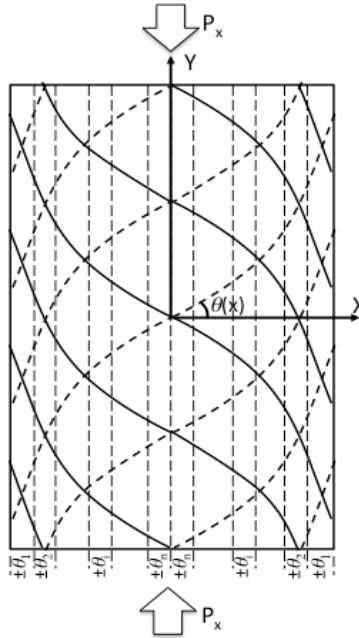
Figure 1. Fibre path definition of the VAT panel. θ_i is the fibre orientation angle in each strip for a VAT

ply. The compressive load P_x is applied as uniform end-shortening.
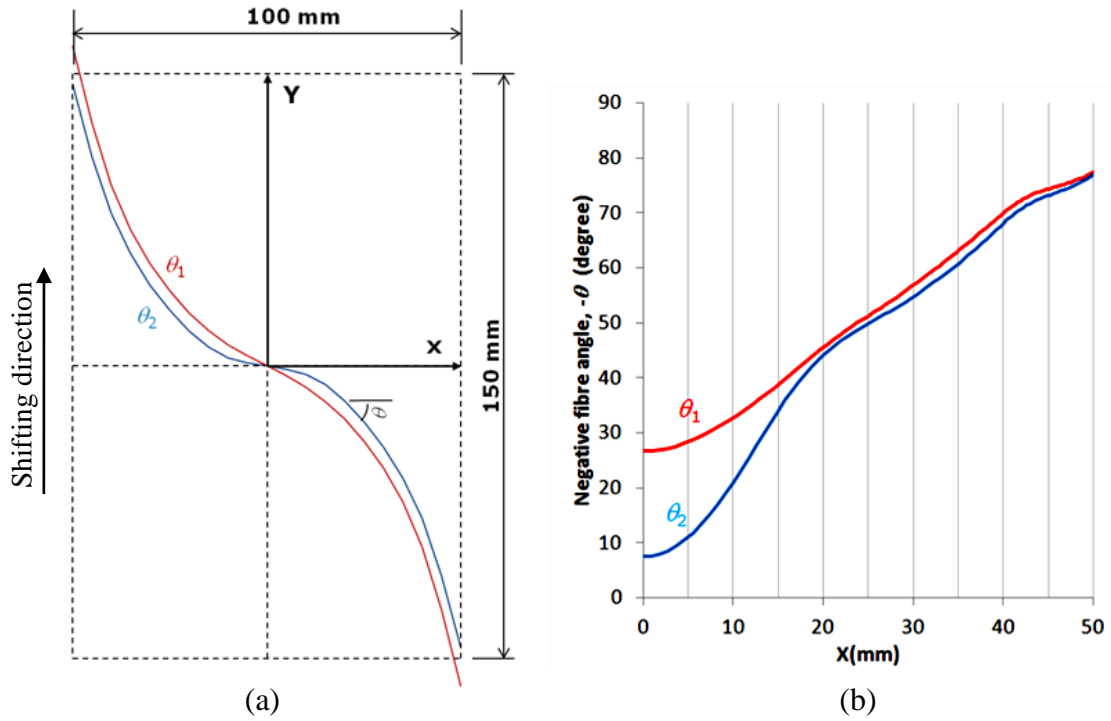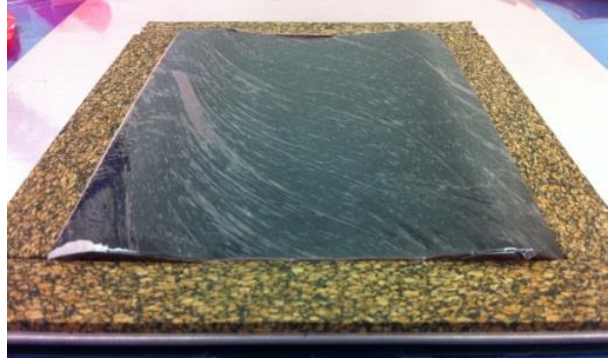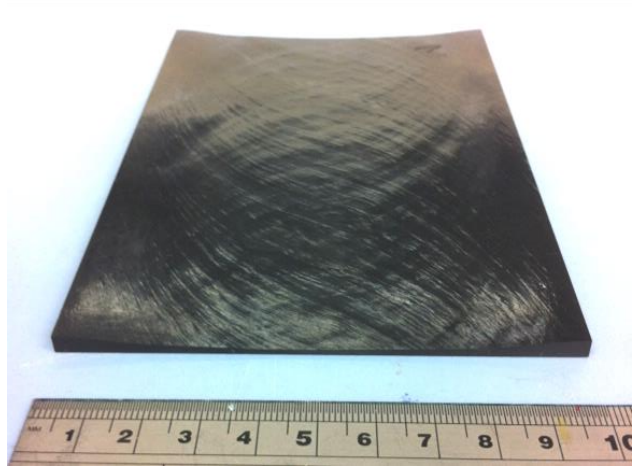
(a)   (b)

Figure 2. VAT composite panel design with a stacking sequence of $[\theta_1/-\theta_1/-\theta_2/\theta_2]_s$; a) Reference tow paths; b) Fibre angle distributions across the half width.

Figure 3. Manufacturing process using VAT prepregs; a) A single VAT prepreg ply after edges have been trimmed using a ply cutter; b) Manual stacked plies; c) Cured VAT panel.

Z_k
Y_k
X_k
h_k
z
Y
X
M_K
∂M_k^u
∂M_k^l

c. Magnified view of A

Mapping

View A

a. Laminate with constant thickness

b. VAT Laminate with thickness variation
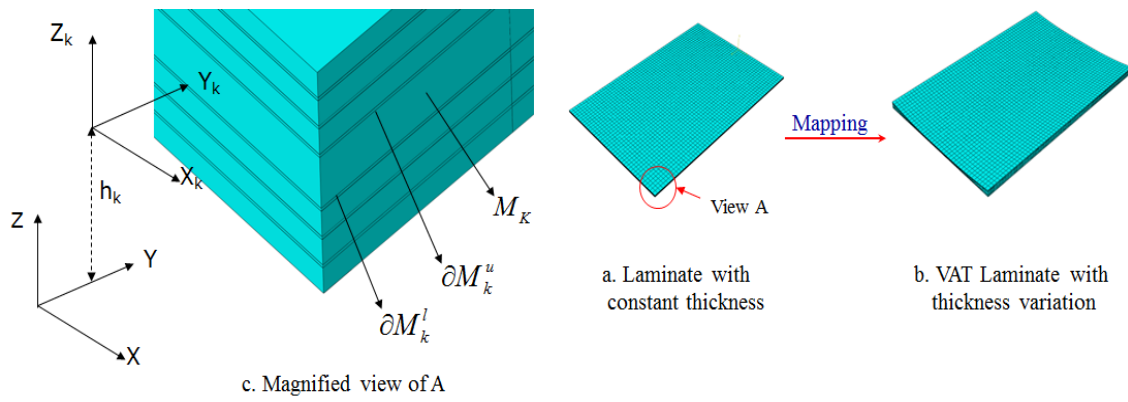
Figure 4. Modelling of as manufactured geometry of VAT laminates.

VAT laminate specimen

a. Setup for Drop Tower impact test

A

View A

b. 3-D impact model for VAT laminate
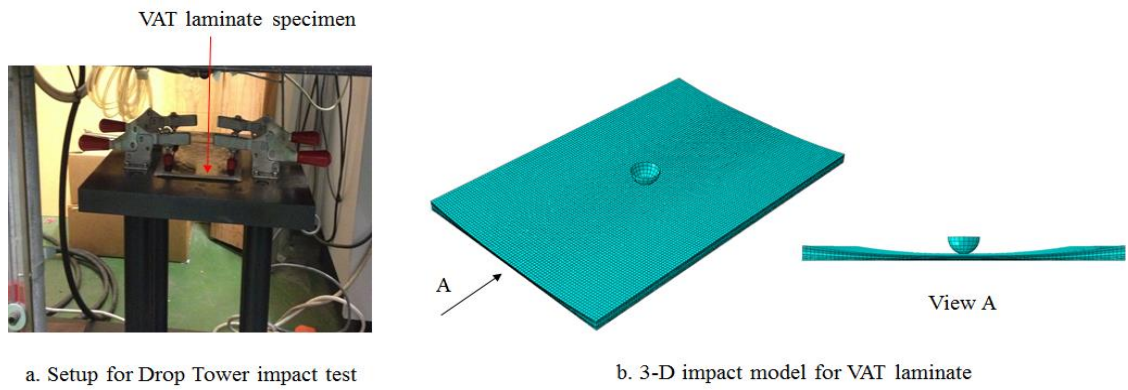
Figure 5. Drop Tower impact setup and 3-D impact model for VAT laminate.
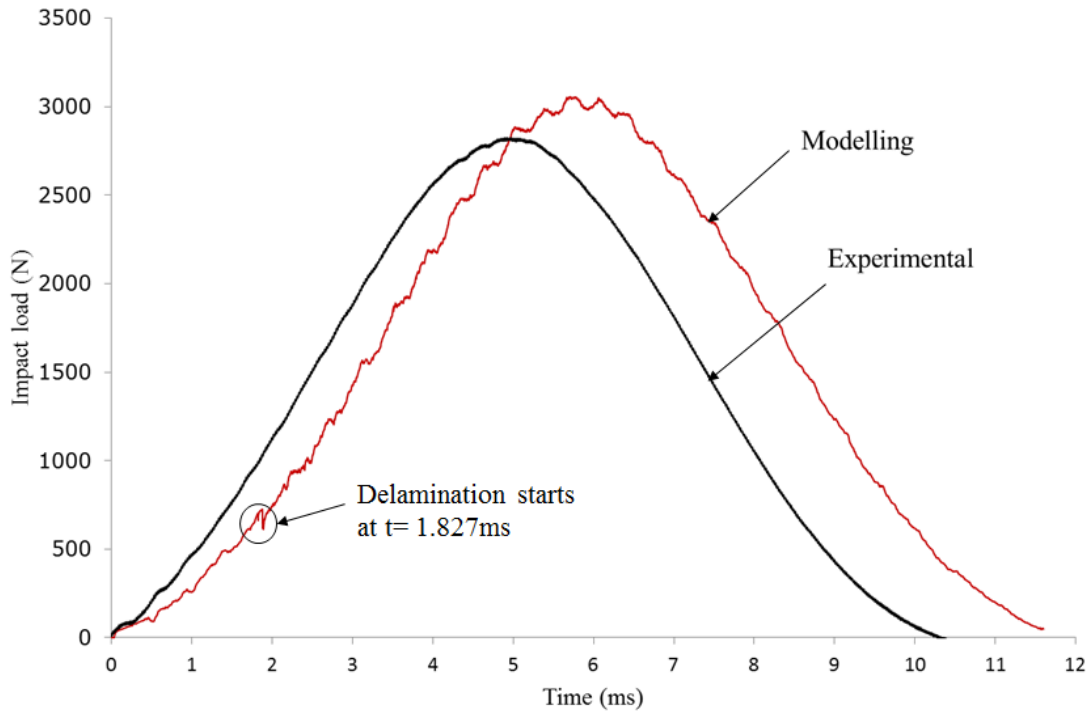
Figure 6. Comparison between the predicted and experimental force–time curves for the VAT laminate with the impact energy of 6 *J* and the impact velocity of 1.3744m/s. Delamination propagation happens at 1.827 *msec* after contact takes place.
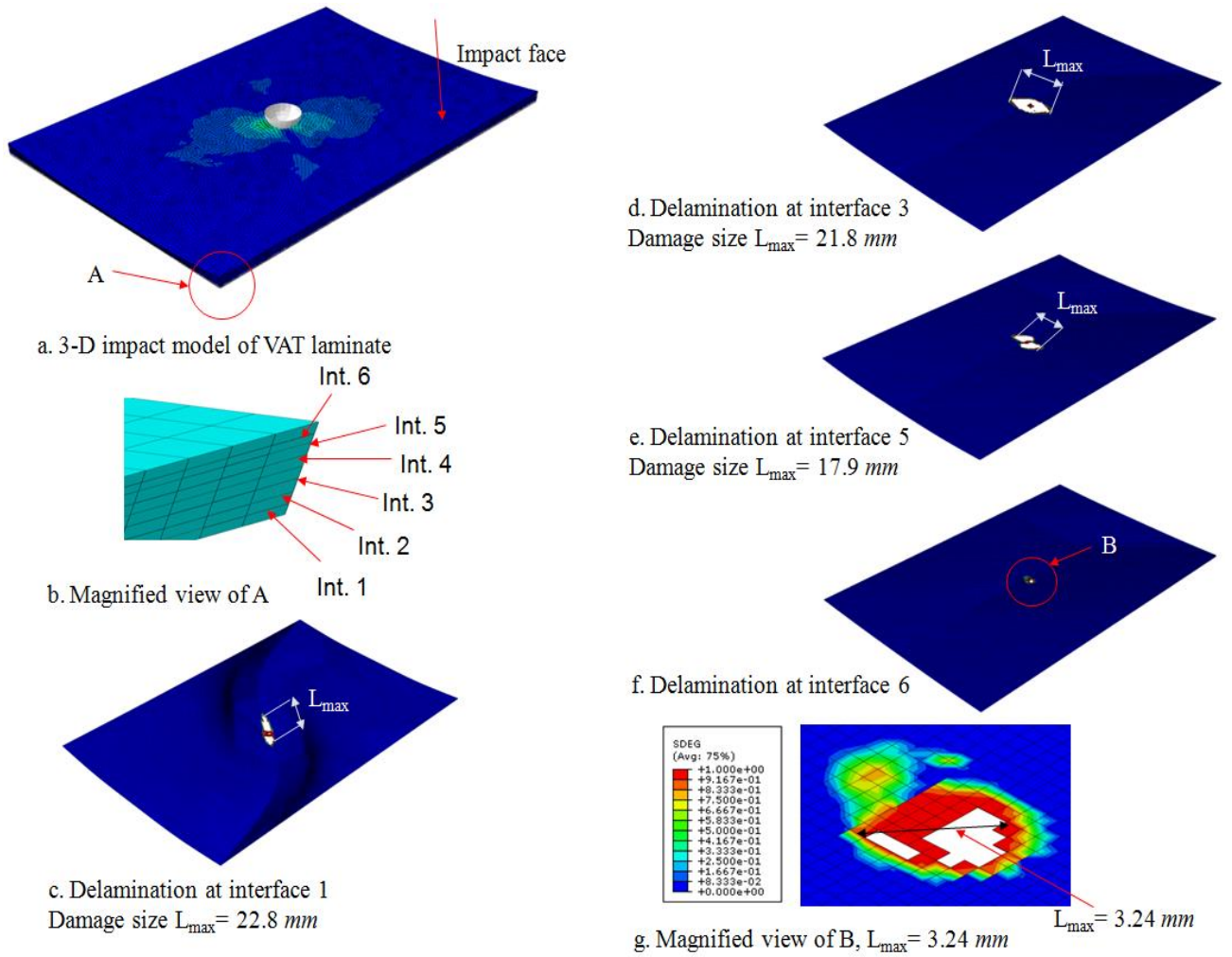
Figure 7. Delamination morphology predicted by the impact model for the VAT laminate with an impact energy of 6 *J* and impact velocity of 1.3744m/s.
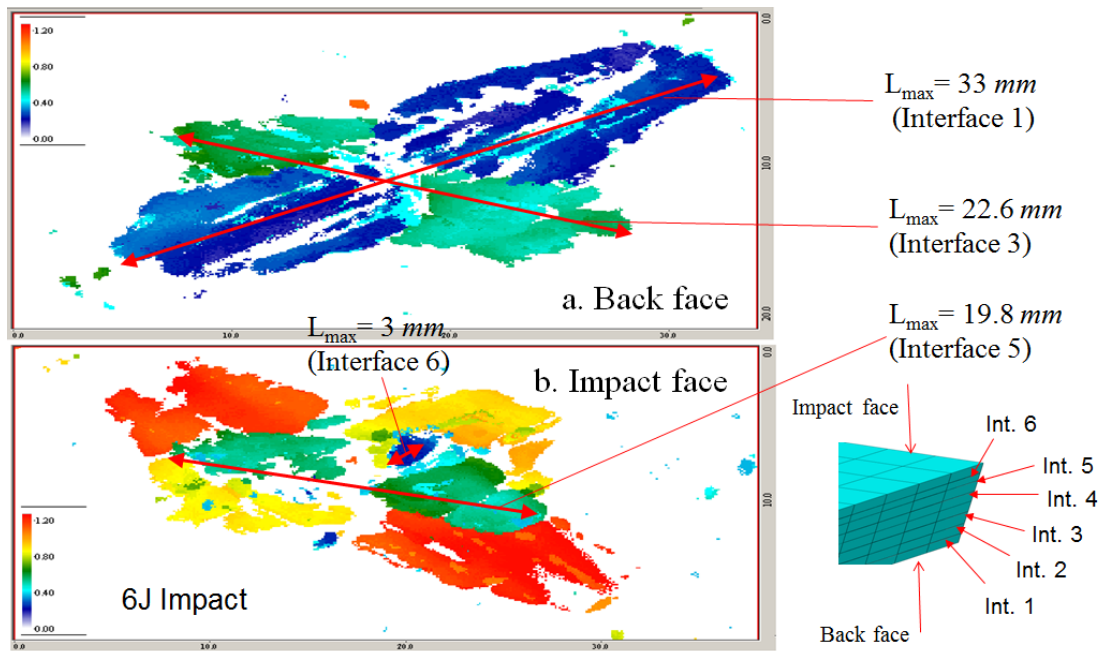
Figure 8. Delamination morphology obtained from the impact test using C-scan for the VAT laminate

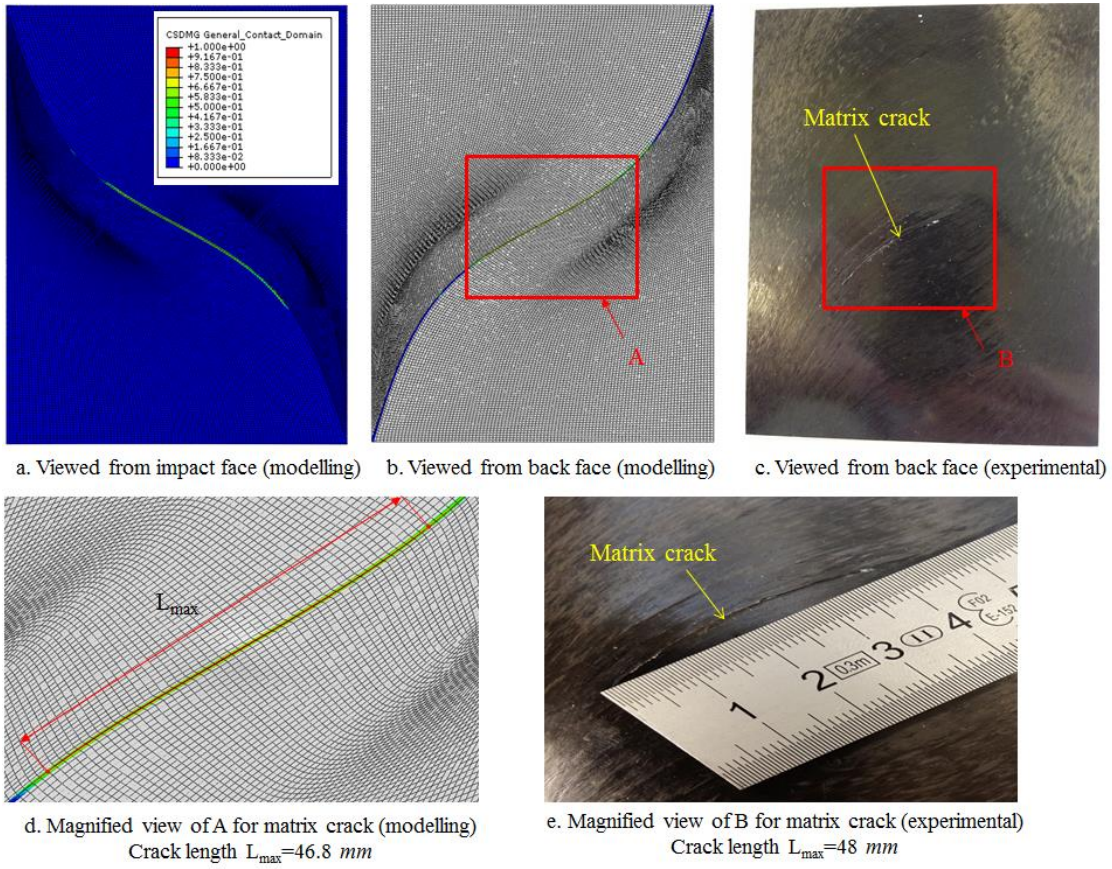with the impact energy of 6 *J* and the impact velocity of 1.3744m/s.

a. Viewed from impact face (modelling)　　b. Viewed from back face (modelling)　　c. Viewed from back face (experimental)

d. Magnified view of A for matrix crack (modelling)
Crack length L_{max}=46.8 mm

e. Magnified view of B for matrix crack (experimental)
Crack length L_{max}=48 mm

Figure 9. Tensile crack propagation in the bottom composite layer predicted by the impact model and the impact test for the VAT laminate with the impact energy of 6 J and the impact velocity of 1.3744m/s.
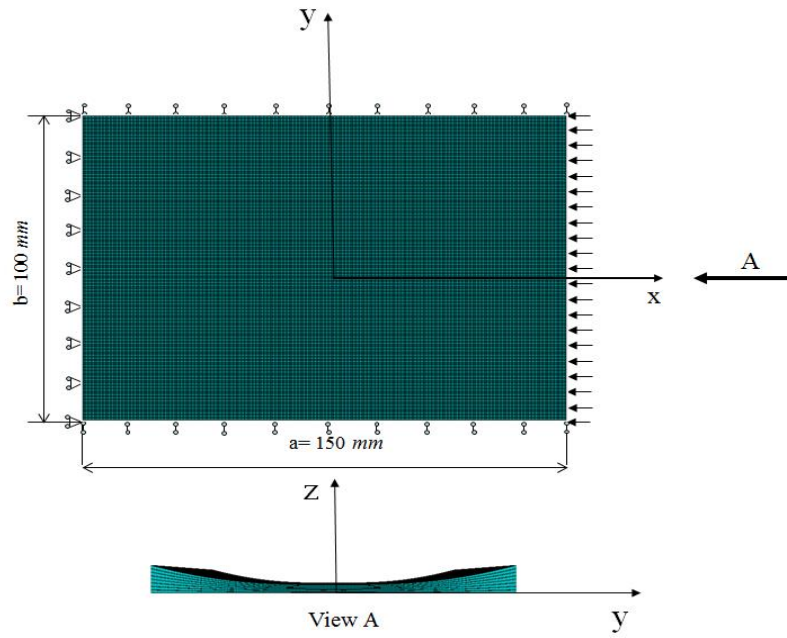
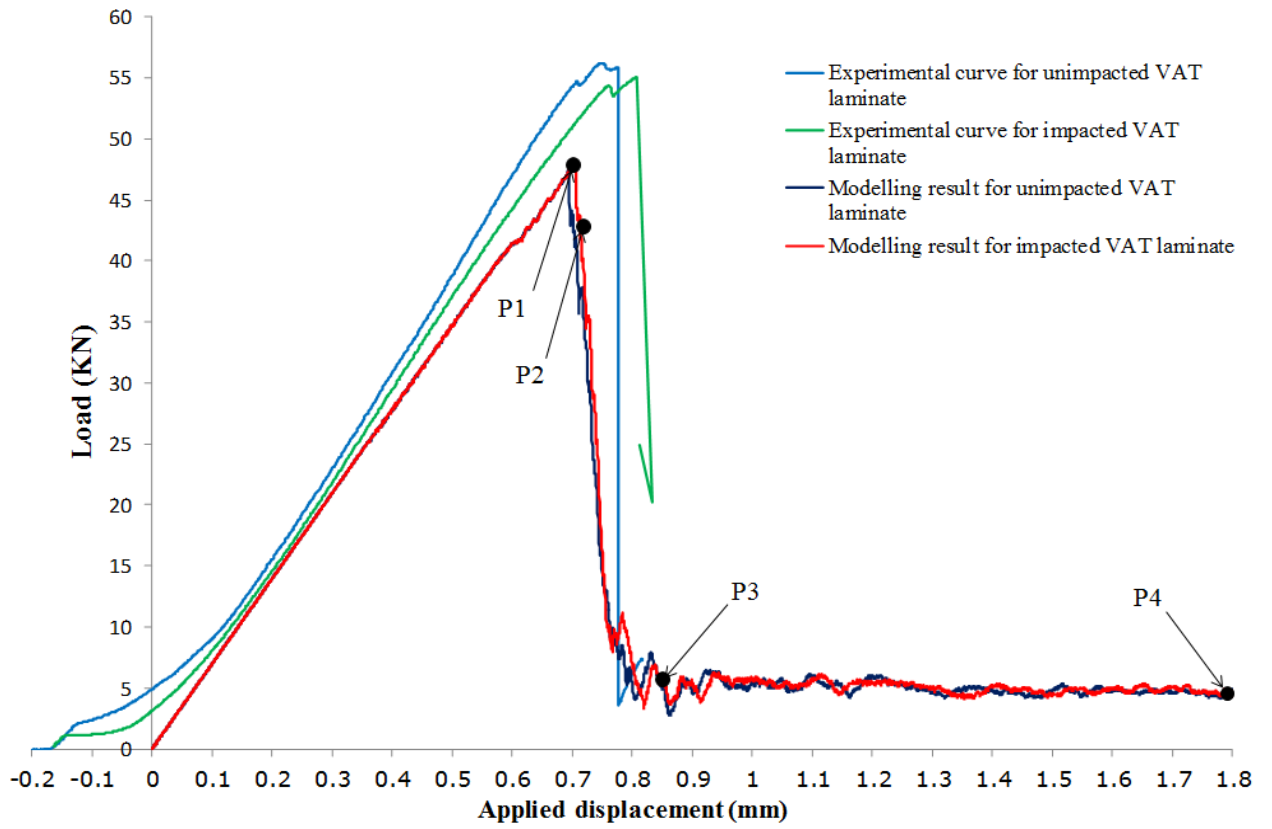**Figure 10.** CAI modelling and CAI test setup for the VAT laminate.

Figure 11. Comparison of force-displacement curves obtained from the CAI modelling and the CAI test for the VAT laminate.

At point P1:
u = 0.699 mm
F = 47.379 KN

At point P2:
u = 0.714 mm
F = 40.648 KN

At point P3:
u = 0.849 mm
F = 5.06 KN

At point P4:
u = 1.8 mm
F = 4.731 KN

a. Damage propagation for unimpacted VAT laminate
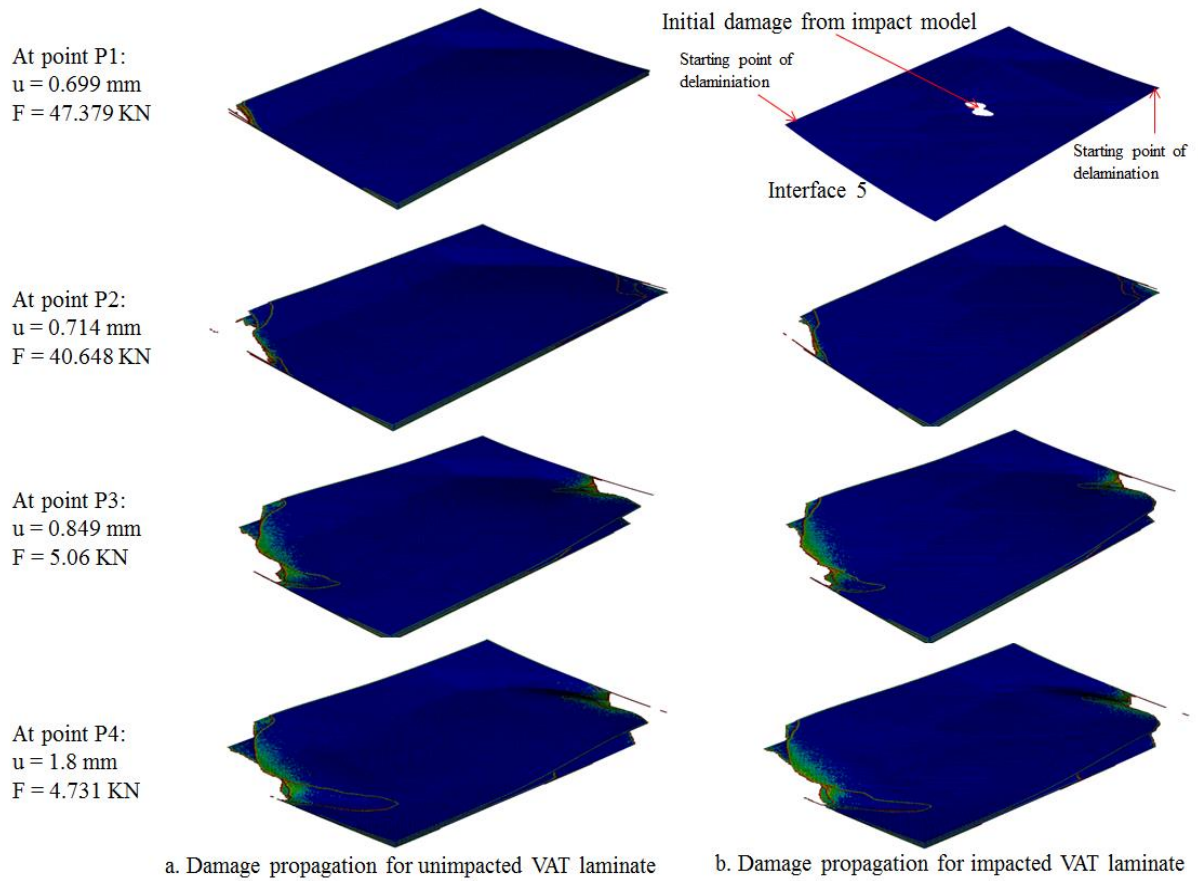
b. Damage propagation for impacted VAT laminate

Figure 12. Delamination growth at different applied displacements of the VAT laminates with consideration of damage propagation. Delamination start at u=0.699*mm* (P=47.379 *KN*) in the interface 5 for the impacted VAT laminate, and at u=0.683*mm* (P=46.445 *KN*) in the interface 5 for the unimpacted VAT laminate.
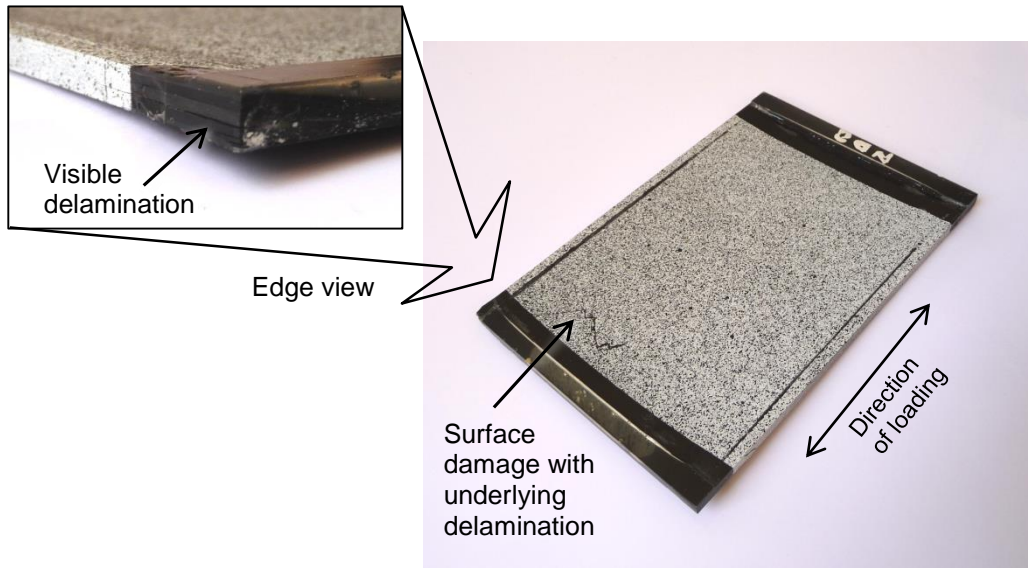
Figure 13. Images of unimpacted VAT laminate after CAI testing, showing delamination in the same

location as predicted.